



Directional Acoustic Wave Manipulation by a Porpoise via Multiphase Forehead Structure

Yu Zhang,^{1,2,*} Zhongchang Song,¹ Xianyan Wang,³ Wenwu Cao,^{4,†} and Whitlow W. L. Au⁵

¹Key Laboratory of Underwater Acoustic Communication and Marine Information Technology of the Ministry of Education, College of Ocean and Earth Sciences, Xiamen University, Xiamen 361005, China

²State Key Laboratory of Acoustics, Institute of Acoustics, Chinese Academy of Sciences, Beijing 100190, China

³Third Institute of Oceanography, State Oceanic Administration, Xiamen 361005, Fujian, China

⁴Department of Mathematics and Materials Research Institute, The Pennsylvania State University, University Park, Pennsylvania 16802, USA

⁵Institute of Marine Biology, University of Hawaii, 46-007 Lilipuna Road, Kaneohe, Hawaii 96744, USA
(Received 11 January 2017; revised manuscript received 17 October 2017; published 1 December 2017)

Porpoises are small-toothed whales, and they can produce directional acoustic waves to detect and track prey with high resolution and a wide field of view. Their sound-source sizes are rather small in comparison with the wavelength so that beam control should be difficult according to textbook sonar theories. Here, we demonstrate that the multiphase material structure in a porpoise's forehead is the key to manipulating the directional acoustic field. Computed tomography (CT) derives the multiphase (bone-air-tissue) complex, tissue experiments obtain the density and sound-velocity multiphase gradient distributions, and acoustic fields and beam formation are numerically simulated. The results suggest the control of wave propagations and sound-beam formations is realized by cooperation of the whole forehead's tissues and structures. The melon size significantly impacts the side lobes of the beam and slightly influences the main beams, while the orientation of the vestibular sac mainly adjusts the main beams. By compressing the forehead complex, the sound beam can be expanded for near view. The porpoise's biosonar allows effective wave manipulations for its omnidirectional sound source, which can help the future development of miniaturized biomimetic projectors in underwater sonar, medical ultrasonography, and other ultrasonic imaging applications.

DOI: [10.1103/PhysRevApplied.8.064002](https://doi.org/10.1103/PhysRevApplied.8.064002)

I. INTRODUCTION

Toothed whales and bats both possess sophisticated biosonar for detecting and tracking prey in a blind and noisy environment [1–4]. Their echolocation signals are directional within a certain frequency range, and the beam pattern may be dynamically adjusted when approaching prey. Physical processes in the beam formation of bats have been recently revealed [5,6]. In comparison, the ultrasonic wave generation and beam control of cetaceans' biosonars are still not well understood.

Dolphins and porpoises have evolved for millions of years to have unique biosonars due to environmental and physiological demands. Au *et al.* found that dolphins possess an automatic gain control [3], and they can locate several centimeter-size objects 100 meters away and discriminate underwater objects with different material properties [7]. Because of the significant difference in acoustic impedance between noseleaf and air, bats utilize irregular baffle geometry for beam forming [4–6], while the

dolphin tissues have acoustic impedance close to that of water, making related wave phenomena more complicated [8,9], such as the generation of interfacial waves [10]. Besides, the porpoise and dolphin's forehead complex, including air sacs, melon, and skull, etc., is rather inhomogeneous with strong gradient properties [11–13]. The respective roles of air sacs, melon, and skull in controlling beam formation have been investigated for both dolphins and porpoises [10,14–16]. The skull and air components serve as strong and important sound reflectors in sound propagations and beam formation for the species and the melon works as a waveguide. Never before have these forehead structures been considered as a whole, and as a natural gradient index (GRIN) material. It is meaningful to investigate how the toothed whales use the impedances between forehead air components and soft tissues, skull structures and soft tissues, to efficiently manipulate their sounds to form dynamic beams to echolocate. Porpoises and dolphins employ these similar forehead acoustic structures to manipulate sounds and form sound beams, but the acoustic structures or the head morphologies are different across the species [7,14–16]. For instance, dolphins, e.g., bottlenose dolphins (*Tursiops truncatus*), have a rostrum tip, which extends forward, but porpoises have no rostrums [7]. The proportions of the acoustic structures in

*Corresponding author.
yuzhang@xmu.edu.cn

†Corresponding author.
dzk@psu.edu

the forehead differ among toothed whales, which leads to a difference of the structures' roles in respective beam formation [14–16]. But it seems these differences among the species do not prevent the species from forming efficient sound beams in respective ways. The investigation into their sound manipulation and sound-beam formation can provide a reference to alternative designs in man-made sonar systems. And an application is exemplified by mimicking the Yangtze finless porpoise's melon to design a directional biomimetic projector [17], which implies that the future application of man-made sonar systems can benefit from dolphins and porpoises, and could help researchers to design artificially structured gradient index materials to improve acoustic imaging and energy flow manipulation [18,19].

The finless porpoise (*Neophocaena phocaenoides*) produces echolocation clicks [20,21] to track prey along the Indo-Pacific coastal waters and some inhabit freshwater estuaries and inlets [22]. The capability of a porpoise using its biosonar system to discriminate the material and size of a target has been experimentally revealed [23]. However, to date, the acoustic structures of the finless porpoise and the way they control acoustic beams have not been well studied. Using an integrated scheme which consists of anatomical imaging, signal analysis, and numerical simulations, we investigate how the forehead of a porpoise, as a multiphase (bone-air-tissue) structure, manipulates acoustic waves. Computed tomography (CT) and tissue measurements are conducted to obtain the sound source and to demonstrate that the porpoise's forehead is actually a natural GRIN material. The porpoise's echolocation click signals are analyzed to provide information for the theoretical modeling. Theoretical models are developed to simulate the impacts of natural GRIN materials on wave propagations and beam patterns. In this study, the forehead acoustic structures of a species of the toothed-whale family is regarded as a natural GRIN material and we study how the compression of this natural GRIN material influences sound manipulation and beam formation. Our results explore the physical principles employed by porpoises and dolphins to manipulate the emitted sound energy.

II. METHODS

A. Computed tomography (CT) scanning and tissue experimental measurements

Porpoises generate and control acoustic beams with complex biological morphology in order to detect a target, as illustrated in Fig. 1. To obtain sound velocity (c) and density (ρ) distributions within the porpoise's head, we perform CT scanning and tissue experiments. A female finless porpoise (*N. a. sunameri*) with the body length of 1.32 m and the weight of 54.0 kg was found dead at the sea near Huian, Fujian Province, China on April 2, 2014.

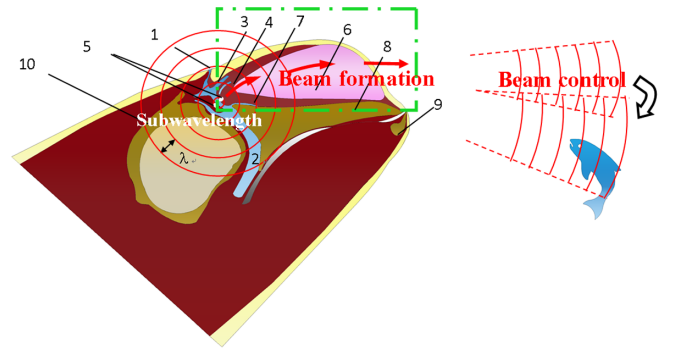


FIG. 1. Illustration of acoustic wave manipulation of a porpoise with biological morphology: (1) blowhole, (2) nasal passage, (3) vestibular sacs, (4) tubular sac, (5) phonic lips (as subwavelength sound source), (6) melon, (7) premaxilla sacs, (8) rostrum, (9) mandible, (10) cranium, where λ is the wavelength, the circles represent the omnidirectional wave produced by the subwavelength source, and the region bounded by the dashed lines represents the forehead complex.

The porpoise was immediately transported for CT scanning with a 0.625-mm slice width (GE Healthcare Lifesciences, Pittsburgh, Pennsylvania) after its discovery. The scanning helps to obtain the CT numbers, which is the Hounsfield unit (HU) of the head structures. During the CT scanning, x rays penetrate the head and the attenuation coefficients of the aforementioned head structures are obtained. These coefficients are compared to that of water to get the structures' HUs. Furthermore, we transversely section the specimen along its body axis from anterior to posterior into 11 slices. Sound velocity of each tissue sample is measured by using an ultrasound velocimeter at room temperature (25 °C) using the method described in our previous work [13]. The ratio between each tissue sample's mass and volume is obtained to determine the density.

B. Field experiments of acoustic signal recording in Xiamen Bay

We determine signal characteristics of the porpoises by recording their echolocation clicks in field experiments. In July 2014, the field experiment was conducted using one 20-m-long diesel power vessel, typically traveling at the speed of 13–15 km/h for three days in Xiamen Bay and adjacent waters in the western coast of the Taiwan Strait, China. A towed hydrophone (8103, Bruel & Kjeer, Neerum, Denmark) with a preamplifier (2635, Bruel & Kjeer, Denmark) is employed to record the porpoise signals. The click signals of porpoises are then gathered into a computer by the DAQ Card (6216, NI, USA). The sampling rate is set as 400 kHz, and an 8th-order butterworth high-pass filter with the cutoff frequency of 5 kHz is used to filter the low-frequency noise. The vessel is powered off when a porpoise is in sight to avoid interference.

C. Acoustic beam simulation of the porpoise model

Based on the CT scanning results and signal recordings, we build a numerical model, shown in Fig. 1, to simulate the physical processes of biosonar emission and beam control in the porpoise's head. In the fluid media (such as air, water, melon, and other soft tissues), only longitudinal waves will propagate, which satisfies the wave equation

$$\frac{1}{\rho_0 c_s^2} \frac{\partial^2 p}{\partial t^2} + \nabla \cdot \left(-\frac{1}{\rho} \nabla p \right) = 0, \quad (1)$$

where p is the sound pressure, ρ_0 is the density, and c_s is the sound velocity. A variable density ρ is included in the equation because the forehead complex is inhomogeneous. In solid skull structures, both shear and compressional waves should be considered as

$$\rho \frac{\partial^2 \mathbf{v}}{\partial t^2} = (\lambda + \mu) \nabla (\nabla \cdot \mathbf{v}) - \mu \nabla^2 \mathbf{v}, \quad (2)$$

where \mathbf{v} is the velocity vector, λ and μ are two Lamé constants, characterizing compression and shear moduli of the skull, respectively. The acoustic fields are numerically derived by solving these wave equations with proper boundary conditions using the finite element method in our previous study [10], where the sound velocity and density of the tissues are obtained from the CT imaging and tissue experiments. The boundary conditions require that the sound pressure and normal velocity at the contact boundary of the fluid media are continuous, while the normal velocity and mechanical stress at the rostrum-tissue boundary are continuous.

In this paper, numerical computations are presented in both time and frequency domains. In the time domain, the sound propagation and acoustic field can be observed clearly, while in the frequency domain, the beam pattern can be visualized in more detail for a given frequency. In the transient time-domain computation, we put a short-duration pulse, with a given formula shown below at the source locations of the models, as sound-source excitation.

$$Q_m = A_0 e^{\alpha_0 t} \sin 2\pi f_0 t, \quad 0 \leq t \leq t_0, \quad (3)$$

$$Q_m = A_1 e^{(-\alpha_1 t + \alpha_2 t_1)} \sin 2\pi f_0 t, \quad t_0 \leq t \leq t_{\text{end}}, \quad (4)$$

where A_0 and A_1 are amplitudes, and f_0 is the peak frequency of the signal, α_0 , α_1 , and α_2 are the attenuation parameters to control the bandwidth of the pulse, t_0 quantitatively expresses the time from signal onset to peak amplitude, t_{end} is the terminal time of the signal and describes the time from the signal peak amplitude to the end, and t is time. In the transient time-domain computation, the f_0 is set as 125 kHz.

To compute in the frequency domain, we put an interior normal acceleration a_n to serve as the sound source in the

model. The equation for the interior normal acceleration can be written as

$$\mathbf{n} \cdot \left[\frac{1}{\rho_0} (\nabla p) \right] = a_n, \quad (5)$$

where \mathbf{n} is the outward-pointing unit normal vector seen from inside the acoustic domain.

III. RESULTS

High-resolution CT imaging visualizes the three-dimensional anatomy and extracts the multiphase structures, including air sacs (vestibular, tubular, and premaxilla sacs), melon, and skull (cranium, mandible, maxilla, teeth), as shown in Fig. 2(a). Phonic lips are small elliptical structures of the fatty bursas and the associated monkey lips–dorsal bursae complex embedded in the nasal system, whose clapping has been well known to generate sounds [7,11]. The phonic-lip geometry is illustrated in the inset by using a Lagrange interpolation algorithm [9]. The size of the phonic lip is estimated to be about 5 mm, while the wavelength in surrounding tissues is 11.5 mm for the frequency of 131 kHz. The skull is a bony structure, air sacs are subject to shape deformation, and the melon is an adipose soft tissue that can be deformed by muscle motion. The HU, density, and sound-speed distributions of a sagittal section are shown in Figs. 2(b), 2(c), and 2(d), respectively.

For the total of 28 tissue samples, the relationships of HU vs sound velocity and HU vs density are derived using linear-regression analysis, as shown in Fig. 2. From the linear relationships between HU vs sound velocity and HU vs density, the distributions of these parameters within the porpoise's head are reconstructed based on the CT and ultrasound measurements. Each slice is cut into smaller samples for c and ρ measurements, as indicated in Fig. 2(b), where the HU is shown by the gray scale and the sixth slice is cut into seven samples. Linear-regression analysis reveals the positive correlation of $c = 2.33 \text{ HU} + 1528.25$ ($R^2 = 0.85$, $p < 0.001$) and the positive correlation of $\rho = 1.03 \text{ HU} + 1005.46$ ($R^2 = 0.81$, $p < 0.001$) as shown in Fig. 2(e). The distributions of ρ and c in the sagittal cross sections are illustrated in Figs. 2(c) and 2(d), respectively. Clearly, the forehead has multiphase GRIN properties of sound velocity and density. Air sacs have the lowest sound velocity, while the skull has the highest sound velocity. Sound-velocity profiles of the eleventh and sixth slices are given in Fig. 2(f), which shows a low sound-velocity core within the melon enclosed by the connective tissues of higher sound velocity. Sound velocity of the forehead tissues is positively correlated with the density ($p < 0.001$), which is not considered in the biomimetic projector design [17]. The physical measurements and CT scanning are combined to prove that the forehead structures are actually natural GRIN materials. It provides

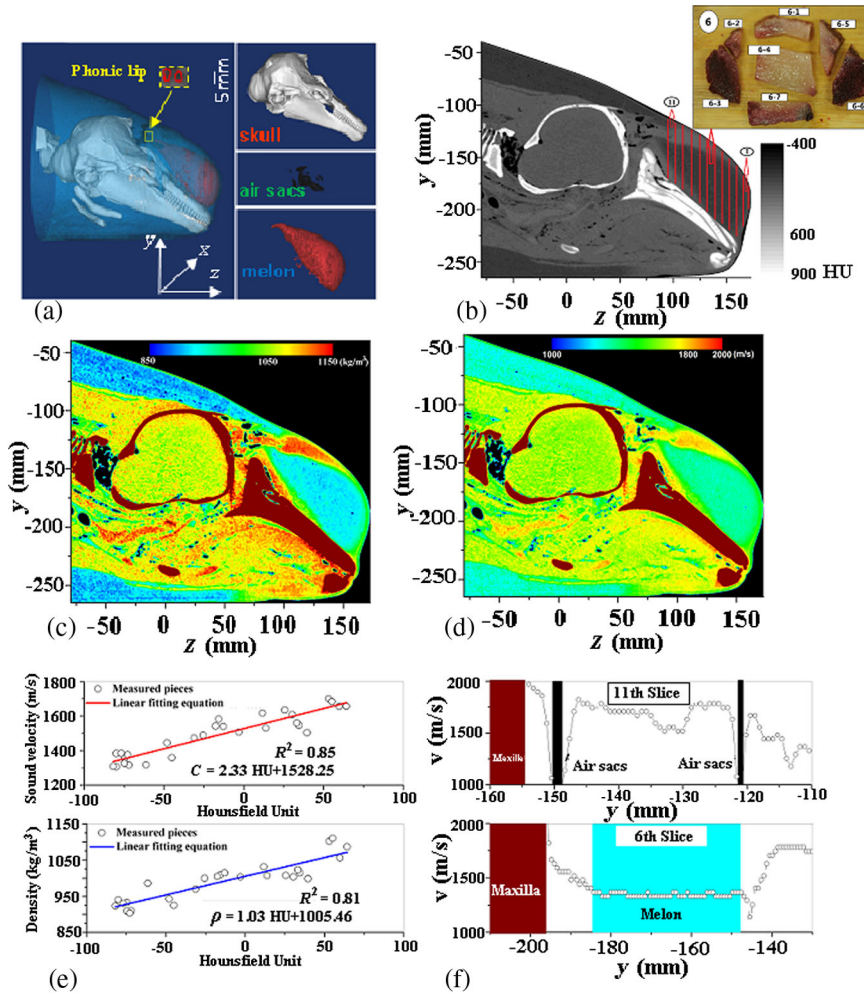


FIG. 2. Multiphase acoustic structures of the porpoise. (a) 3D visualization of anatomy of the porpoise's head by CT scanning. Phonic lips are shown in the inset. Skull, air sacs, and melon constitute a multiphase complex. (b) Sagittal cross section of the head, where the forehead is dissected transversely into eleven slices and six tissue pieces are cut from the sixth slice. The labels of the tissue pieces are also given. (c) Density distribution. (d) Sound-velocity distribution. (e) Linear-regression relationships of HU vs sound velocity and HU vs density. (f) Sound-velocity profiles of the eleventh and sixth slices.

the fundamental principle for applying artificial GRIN materials to mimic the biosonar of the porpoise.

During the field experiment, a total of 96 clicks are recorded for analysis as shown in Fig. 3(a). A click train of 14 clicks with the signal-to-noise ratio higher than 10 dB and the corresponding frequency spectra are shown in Figs. 3(b) and 3(c), where clicks are numbered in the order of occurrence. Figure 3(d) gives the distributions of the peak frequencies and the bandwidths at -3 -dB for the 96 clicks. The peak frequency ranges from 121 to 140 kHz with the mean value and standard deviation of 130.9 ± 4.3 kHz. The -3 -dB bandwidth varies from 7.0 to 16.0 kHz with the mean value and standard deviation of 10.7 ± 2.1 kHz. Differing from the amplitude, peak frequencies of the click train show less variation.

Based on the CT imaging, physical measurements, and acoustic signal recordings, we construct numerical models to simulate the wave propagations and ultrasound beams of the porpoise. Wave propagations within the porpoise's head are shown in Fig. 4(a), where I, II, III, and IV correspond to the propagation time at 0.05, 0.11, 0.15, and 0.25 ms, respectively. Figures 4(b) and 4(c) compare the simulated waveform and spectrum of the on-axis signal with those of

the real click data recorded. Good agreement is found in the normalized scale. Because of diffraction, the subwavelength source produces the cylindrical wave $p_{\text{sub}}(r) \sim e^{-jkr}/\sqrt{r}$ in the two-dimensional y - z plane, where r represents the distance from the source. However, the porpoise's multiphase structures induce complicated processes: air sacs together with the nasal passage as the sound reflector and scattering structure prevent sound from propagating backward. The melon as a GRIN structure guides the refracted wave toward its central region. The fluid-solid coupling between skull and tissues generates interfacial waves [10]. In the far field, the wave can be described as $p_{\text{por}}(r, \varphi) = \iint [(p_s e^{-jkr})/\sqrt{r}] dy dz \sim D(\varphi) e^{-jkr}/\sqrt{r}$ [5,7], where $p_s(y, z)$ is the pressure per unit area on the porpoise's structure, $D(\varphi)$ denotes the directivity that can be numerically obtained by $D(\varphi) = p_{\text{por}}(r, \varphi)/p_{\text{por}}(r, 0)$, where $p_{\text{por}}(r, 0)$ is the main-lobe pressure, and φ represents the angle with respect to the horizontal direction. Figure 4(d) shows the directivities of the subwavelength sources with and without the porpoise's structure, where the source length is set to 5 mm according to Fig. 2(a). Therefore, multiphase structures of the porpoise's forehead collectively convert

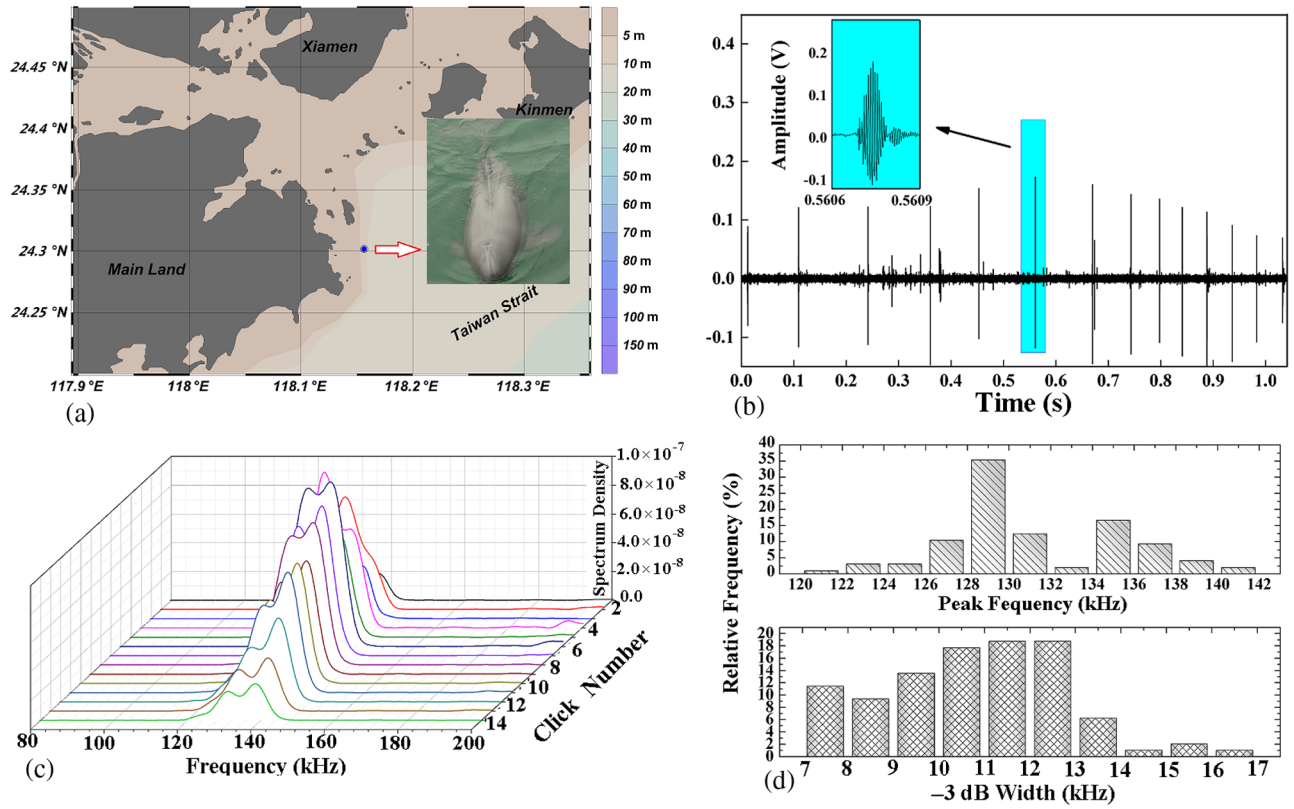


FIG. 3. Acoustic signal characteristics of the porpoise. (a) Experimental site in Xiamen Bay, China, where the blue dot near the coast indicated the recording location. Waveforms (b) and frequency spectra (c) of a click train recorded. (d) Distributions of the peak frequency and -3 dB bandwidth for the 96 clicks of the porpoise. The frequencies from acoustic recording and structure geometries from CT imaging provide modeling parameters for numerical simulations.

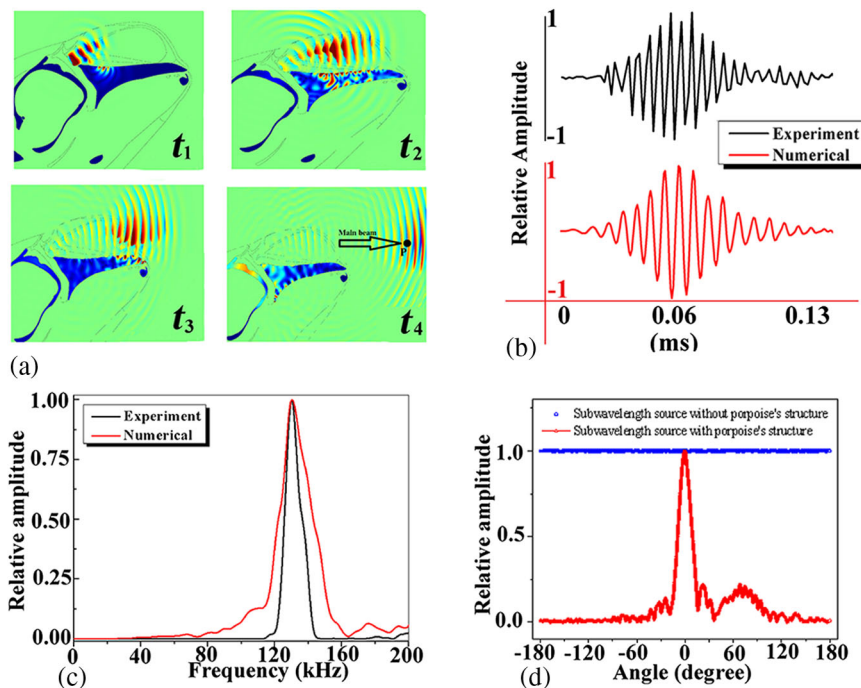


FIG. 4 (a) Acoustic fields of the porpoise model, where I, II, III, and IV correspond to the propagation time at 0.05, 0.11, 0.15, and 0.25 ms, respectively. Waveform and spectrum comparisons between the numerical simulated signal obtained at point P from (a) and a real click recorded are shown in (b) and (c), respectively. (d) The directivities of the subwavelength sources with and without the porpoise's structure.

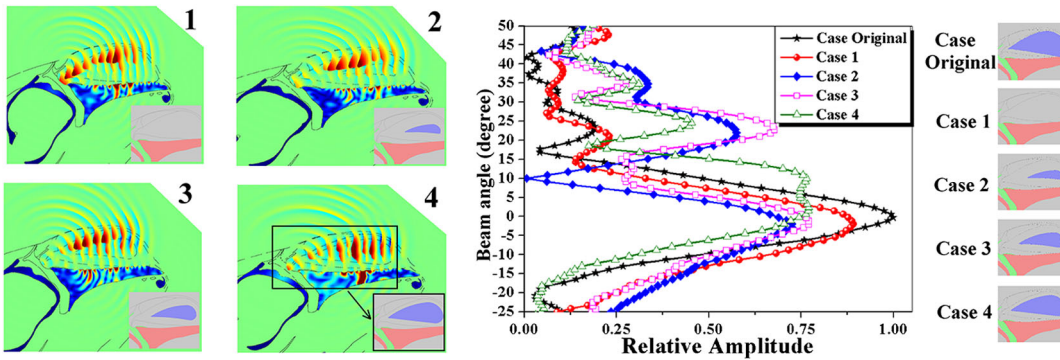


FIG. 5. The effect of the melon size on acoustic field (left) and beam directivities (right), where cases 4 to 1 correspond to the melon size of 75%, 50%, 25%, and 0%, respectively, while the original case represents the original melon without reducing its size.

the omnidirectional wave generated by the subwavelength source into a directional one.

To further demonstrate how the forehead complex manipulates the beam pattern, we exemplify melon and air sacs by changing their size and orientation. Figure 5 compares the sound propagations inside the head and beam directivities at 1 m of the models with different melon sizes, including 100%, 75%, 50%, 25%, and 0% of the original size. Interestingly, directional patterns are observed in all cases, even including the model without melon (case 1). The original case represents the porpoise model with a full set of forehead complex, of which the melon and air sac are not changed. The original model produces a main beam along the vertical direction with a beamwidth of 13.3° . The calculated main beam directions with the melon sizes of 75%, 50%, 25%, and 0% are -1.9° , -2.3° , and -1.6° and 1.9° , respectively, and their corresponding -3 dB beamwidths are 15.8° , 15.2° , 13.6° , and 20.6° . The sidelobe intensities increase with the decrease of the melon size.

Figure 6 shows the effects of orientation and length of the vestibular sac. The model with the vestibular sac orientation angle of 25° has the main beam angle and -3 dB beamwidth of 3.2° and 21.7° , respectively. Both are larger than that of the model result with the orientation angle of 15° (1° and 15.9° , respectively). The orientations seem to widen the

beamwidth of the original model I. For the length of the vestibular sac, the elongation and shortening do not seem to cause as much difference as that of orientation. The elongation of case 3 and shortening of case 4 in Fig. 6 give -3 dB beamwidths of 13.2° and 13.1° , respectively. Therefore, we further combine the orientation of the vestibular sac and the area of forehead fluid structures.

The porpoises have complex facial musculature to induce simultaneous deformations of the melon and air sacs. To simulate this, we apply a sequence of compressing processes I, II, III, IV, and V to the models as shown in Figs. 7 and 8. The normalized area (NA) of the forehead is monotonically decreased from I to V, and the orientation angles of the vestibular sac change by the amount of 0° , 5° , 10° , 15° , and 20° , respectively. Figure 7 compares their wave propagations and acoustic fields, while their directivities, main beam angles, and -3 dB beamwidths are given in Fig. 8. The main beam angle and -3 dB beamwidth change from 0° and 13.3° of model I to 2.2° and 14.2° of model II, 2.7° and 16.5° of model III, 1.5° and 18.4° of model IV, and 1.2° and 19.6° of model V, respectively. The operation of the forehead structures demonstrates the sound-beam patterns are modulated accordingly, suggesting that porpoises have many ways to adjust their beams.

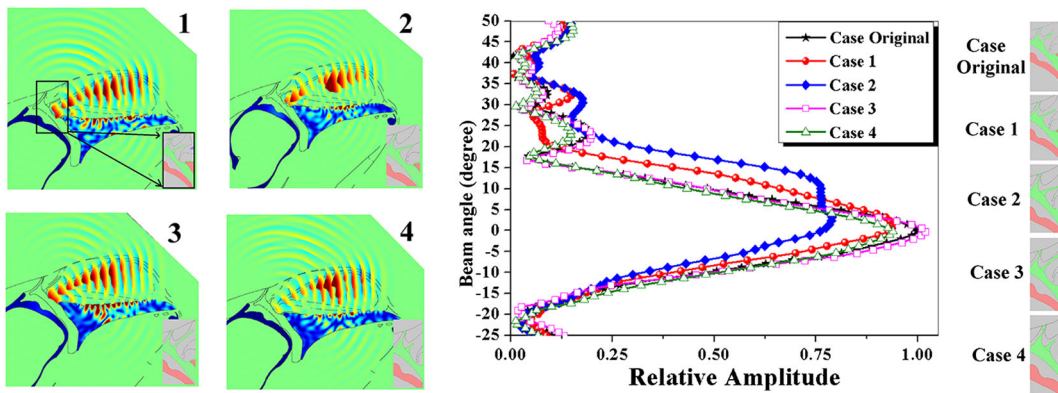


FIG. 6. The effects of length and orientation of the vestibular sac on the acoustic field (left) and beam directivities (right), where cases 1 and 2 correspond to the orientation angle of 15° and 25° in the upper plot, respectively, and cases 3 and 4 correspond to the vestibular sac length of 150% and 50% in the lower plot, respectively.

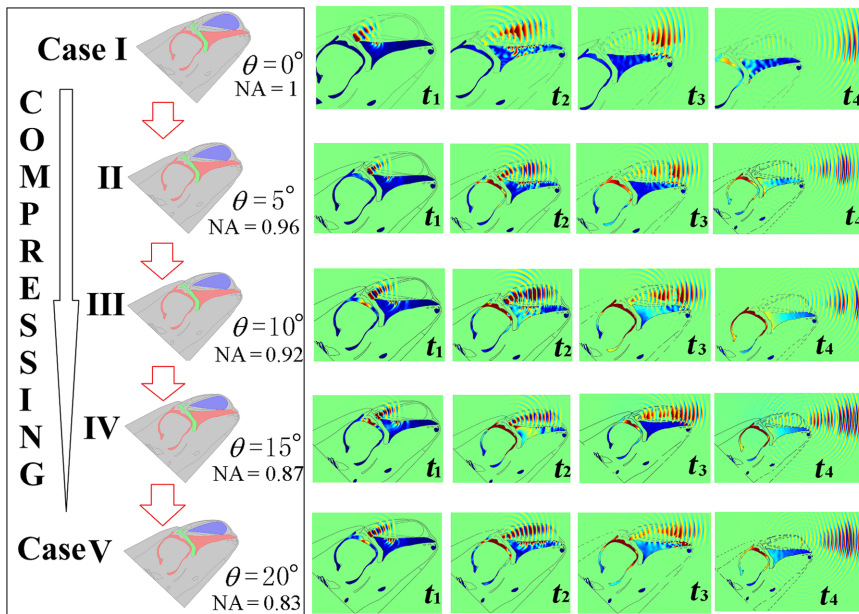


FIG. 7 The compressing effect of models I, II, III, IV, and V, and their acoustic fields inside the head, where θ represents the orientation angle of the vestibular sac and NA represents the normalized area of the forehead tissues with respect to those of the original model I.

IV. DISCUSSIONS

Our results show that the size of the low-sound-speed melon, and the length and orientation of the vestibular sac can impact the beam formation (Figs. 5 and 6), which supports previous numerical [13–16] and the experimental [8] results. More importantly, the air sacs, melon, and skull function jointly produce the desired effects to form sound beams. Larger melons bend waves and suppress the energy levels of sidelobes. Increasing the vestibular sac length would enhance the air-fluid as well as fluid-solid reflections and interfacial wave generations. This further suggests that the forehead structures, to some extent, should be considered as a whole to work as a natural GRIN material to control wave propagations and sound beams.

Ultrasound signal production by the finless porpoise is rather complicated, involving the interaction between biomechanical and acoustic processes. The problem cannot be solved based on simple acoustic analysis. In this study, we use integrated multiple methodologies to identify that the multiphase property of the forehead is the key for directional beam formation and control. CT scanning

reveals complex structures of the porpoise’s forehead, including skull, air sacs, and melon (Fig. 2). The phonic-lip size is about one-half of the sound wavelength in its surrounding tissues, suggesting that the porpoise employs the subwavelength source to emit sounds. Tissue experiments allow measurements of density and sound velocity, which are difficult to be achieved *in vivo*. Numerical simulations show the correlation between internal acoustic structure and external beam pattern. The predicted waveform agrees well with the real porpoise’s signal (Fig. 4). This integrated investigation scheme helps us uncover the biosonar mechanism of the porpoise. The results clearly suggest that the natural GRIN material characteristics of its forehead is the key to form and control directional sound beams. The original source would lead to omnidirectional wave propagations without the porpoise forehead GRIN structure, as shown in Fig. 4(d). When putting the same omnidirectional sound source into the porpoise forehead, the sound beam directivity becomes sharp, with a -3 dB beamwidth of 13.3° . The directivity is augmented by 13.5 times based on the ratio of $180^\circ/13.3^\circ$. This natural GRIN material and the way it manipulates

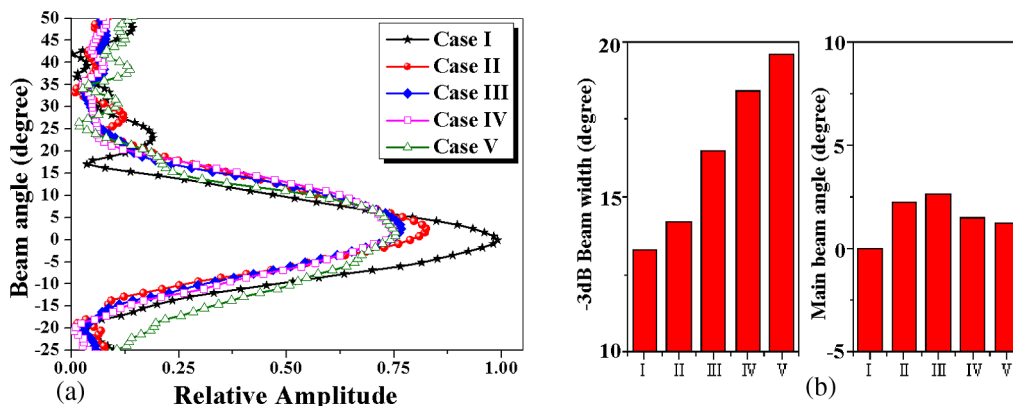


FIG. 8 The beam directivities are shown in (a), while the main beam angle and -3 dB beamwidths are given in (b).

sounds and beam formation in a porpoise are investigated, and the results could provide guidance to man-made metamaterials for the control of sound propagation and enhancing energy emission efficiency. Man-made metamaterials depend on special designs to break traditional limitations [18,19,24–26]. In traditional ways, sound-source emission in low frequencies is hard to realize with both high power and high directivity [25,26]. This requires researchers to design materials with special sound-speed profiles to conquer the limitations above [18,19,24–26]. In comparison, it seems that many odontocetes species have developed a system to emit low-frequency sound beams with high directivity and intensity [1,7,8–10,13–16]. The porpoise, as a species from odontocetes, has been proven to own a natural GRIN material in its forehead, but this species uses high-frequency sounds to echolocate. Therefore, it would be meaningful to further extend the investigation into odontocetes which emit low-frequency sounds. The results of the study of beam control by porpoise using natural GRIN material could be useful for the future development of man-made metamaterials.

Computer modeling in this study offers an efficient way to realize structural deformation and allows us to evaluate its effect on beam patterns. Wisniewska *et al.* [8] found that harbor porpoises could compress their melon to produce wider acoustic beams when targets are at a close range to avoid the targets fleeing from the sonar scan zone. The melon and surrounding tissue functioned as an adjustable lens, and their deformations induced by accessory muscles could change the acoustic path. In Fig. 8, the compressing models produce wider beams, which is in good agreement with experimental observations on harbor porpoises [8]. Previous findings indicate that the harbor porpoises can control their beamwidth when tracking prey, and their ability to present the controls relates to the deformation of the forehead melon and air sacs. The -3 dB beamwidth of the harbor porpoises changed from 9.1° to a maximum of 15.1° . In comparison, the models of the finless porpoise in the current paper give a -3 dB beamwidth change from 13.3° to 19.6° . The beam changes of harbor porpoises come from a joint effect of deformations of forehead melon, muscle, and air sacs, and the distance change from targets to harbor porpoises. The beamwidth changes of the finless porpoise modeled here are caused solely by compressing forehead soft tissues and orientations of the vestibular sac. Even with that consideration, our results indicate that the forehead complex constitutes an important obligato structure of the porpoise, and its shape change can lead to dynamic beam properties.

V. CONCLUSIONS

In this paper, we show that the finless porpoise's forehead as a multiphase (skull-air-tissue) natural GRIN structure is the key to manipulating directional waves. The compression of the forehead complex decentralizes

energy flow and expands the acoustic beam. The melon is not a dominant factor in forming the directional beam, but its role in impacting sidelobe energies is significant. These findings help us better understand how toothed whales manipulate sounds generated from subwavelength sources, which can provide guidance in the development of miniaturized biomimetic sonar systems in the future with a much smaller size, higher resolution, and more freedom in beam control. As a reference, the natural GRIN structures in the porpoise's forehead might enlighten researchers to develop alternative designs to overcome traditional size-wavelength limitations to enhance directional sound emission at low frequencies. The special organization of skull structures, soft tissues, and air components in the porpoise's head could provide a model for developing man-made metamaterials to control sound propagations.

ACKNOWLEDGMENTS

This work is financially supported in part by the National Science Foundation of China (Grants No. 41276040, No. 11174240, and No. 41676023) and the Natural Science Foundation of Fujian Province of China (Grant No. 2012J06010). The Project is also partially sponsored by the Scientific Research Foundation for the Returned Overseas Chinese Scholars, State Education Ministry. The authors also want to thank Professor Minghui Lu and Professor Nicholas Xuanlai Fang for their helpful comments on the manuscript.

-
- [1] W. W. L. Au and J. A. Simmons, Echolocation in dolphins and bats, *Phys. Today* **60**, No. 9, 40 (2007).
 - [2] N. Veselka, D. D. McErlain, D. W. Holdsworth, J. L. Eger, R. K. Chhem, M. J. Mason, K. L. Brain, P. A. Faure, and M. B. Fenton, A bony connection signals laryngeal echolocation in bats, *Nature (London)* **463**, 939 (2010).
 - [3] W. W. L. Au and K. J. Benoit-Bird, Automatic gain control in the echolocation system of dolphins, *Nature (London)* **423**, 861 (2003).
 - [4] L. Jakobsen, J. M. Ratcliffe, and A. Surlykke, Convergent acoustic field of view in echolocating bats, *Nature (London)* **493**, 93 (2013).
 - [5] Q. Zhuang and R. Muller, Noseleaf Furrows in a Horseshoe Bat Act as Resonance Cavities Shaping the Biosonar Beam, *Phys. Rev. Lett.* **97**, 218701 (2006).
 - [6] L. Gao, S. Balakrishnan, W. He, Z. Yan, and R. Muller, Ear Deformations Give Bats a Physical Mechanism for Fast Adaptation of Ultrasonic Beam Patterns, *Phys. Rev. Lett.* **107**, 214301 (2011).
 - [7] W. W. L. Au, *The Sonar of Dolphins* (Springer-Verlag, New York, 1993).
 - [8] D. M. Wisniewska, J. M. Ratcliffe, K. Beedholm, C. B. Christensen, M. Johnson, J. C. Koblitz, M. Wahlberg, and P. T. Madsen, Range-dependent flexibility in the acoustic field of view of echolocating porpoises (*Phocoena phocoena*), *eLife* **4**, 05651 (2015).

- [9] C. Wei, Y. Zhang, and W. W. L. Au, Simulation of ultrasound beam formation of baiji (*Lipotes vexillifer*) with a finite element model, *J. Acoust. Soc. Am.* **136**, 423 (2014).
- [10] Z. C. Song, Y. Zhang, C. Wei, and X. Y. Wang, Inducing rostrum interfacial waves by fluid-solid coupling in a Chinese river dolphin (*Lipotes vexillifer*), *Phys. Rev. E* **93**, 012411 (2016).
- [11] T. W. Cranford, M. Amundin, and K. S. Norris, Functional morphology and homology in the odontocete nasal complex: Implications for sound generation, *J. Morphol.* **228**, 223 (1996).
- [12] M. S. Soldevilla, M. F. McKenna, S. M. Wiggins, R. E. Shadwick, T. W. Cranford, and J. A. Hildebrand, Cuvier's beaked whale (*Ziphius cavirostris*) head tissues: Physical properties, and CT imaging, *J. Exp. Biol.* **208**, 2319 (2005).
- [13] C. Wei, Z. T. Wang, Z. C. Song, K. X. Wang, D. Wang, W. W. L. Au, and Y. Zhang, Acoustic property reconstruction of a neonate Yangtze finless porpoise's (*Neophocaena asiaeorientalis*) head based on CT imaging, *PLoS One* **10**, e0121442 (2015).
- [14] J. L. Aroyan, T. W. Cranford, J. Kent, and K. S. Norris, Computer modeling of acoustic beam formation in *Delphinus delphis*, *J. Acoust. Soc. Am.* **92**, 2539 (1992).
- [15] C. Wei, W. W. L. Au, Z. C. Song, and Y. Zhang, The role of various structures in the head on the formation of the biosonar beam of the baiji (*Lipotes vexillifer*), *J. Acoust. Soc. Am.* **139**, 875 (2016).
- [16] C. Wei, W. W. L. Au, D. R. Ketten, Z. C. Song, and Y. Zhang, Biosonar signal propagation in the harbor porpoise's (*Phocoena phocoena*) head: The role of various structures in the formation of the vertical beam, *J. Acoust. Soc. Am.* **141**, 4179 (2017).
- [17] R. Q. Li, B. Liang, Y. Li, W. W. Kan, X. Y. Zou, and J. C. Cheng, Broadband asymmetric acoustic transmission in a gradient-index structure, *Appl. Phys. Lett.* **101**, 263502 (2012).
- [18] F. Lemoult, G. Lerosey, J. de Rosny, and M. Fink, Resonant Metalenses for Breaking the Diffraction Barrier, *Phys. Rev. Lett.* **104**, 203901 (2010).
- [19] Y. Zhang, X. W. Gao, S. Zhang, W. W. Cao, L. G. Tang, D. Wang, and Y. Li, A biomimetic projector with high subwavelength directivity based on dolphin biosonar, *Appl. Phys. Lett.* **105**, 123502 (2014).
- [20] S. H. Li, D. Wang, K. X. Wang, T. Akamatsu, Z. Q. Ma, and J. B. Han, Echolocation click sounds from wild inshore finless porpoise (*Neophocaena phocaenoides sunameri*) with comparisons to the sonar of riverine *N. p. asiaeorientalis*, *J. Acoust. Soc. Am.* **121**, 3938 (2007).
- [21] S. H. Li, K. X. Wang, D. Wang, S. Y. Dong, and T. Akamatsu, Simultaneous production of low- and high-frequency sounds by neonatal finless porpoises, *J. Acoust. Soc. Am.* **124**, 716 (2008).
- [22] T. A. Jefferson and J. Y. Wang, Revision of the taxonomy of finless porpoises (*genus Neophocaena*): The existence of two species, *J. Mar. Anil. Their. Ecol.* **4**, 3 (2011).
- [23] F. Nakahara, A. Takemura, T. Koido, and H. Hiruda, Target discrimination by an echolocation finless porpoise, *neophocaena phocaenoides*, *Marine mammal science* **13**, 639 (1997).
- [24] X. D. Fan, Y. F. Zhu, B. Liang, J. C. Cheng, and L. K. Zhang, Directional radiation of sound waves by a subwavelength source, [arXiv:1702.07277](https://arxiv.org/abs/1702.07277).
- [25] J. J. Zhao, L. K. Zhang, and Y. Wu, Enhancing monochromatic multipole emission by a subwavelength enclosure of degenerate Mie resonances, *J. Acoust. Soc. Am.* **142**, EL24 (2017).
- [26] D. T. Blackstock, *Fundamentals of Physical Acoustics* (John Wiley and Sons, Hoboken, NJ, 2000).